JOURNAL OF PROPULSION AND POWER
Vol. 20, No. 3, May–June 2004

Experimental Investigation of Separated Nozzle Flows

Craig A. Hunter*
NASA Langley Research Center, Hampton, Virginia 23681

A detailed experimental study of separated nozzle flows has been conducted at the NASA Langley Research Center 16-Foot Transonic Tunnel Complex. As part of a comprehensive static performance investigation, force, moment, and pressure measurements were made and schlieren flow visualization was obtained for a subscale, nonaxisymmetric, two-dimensional, convergent–divergent nozzle. For reference, experimental results were compared with theoretical predictions based on one-dimensional gasdynamics and an approximate integral momentum boundary-layer method. Results from this study indicate that overexpanded nozzle flow was dominated by shock-induced boundary-layer separation, which was divided into two distinct flow regimes: three-dimensional separation with partial reattachment and fully detached two-dimensional separation. The test nozzle was observed to go through a marked transition in passing from one regime to the other. In all cases, separation provided a significant increase in static thrust efficiency compared to the ideal prediction. Results suggest that, with controlled separation, the entire overexpanded range of nozzle performance would be within 16% of the peak thrust efficiency. By offering savings in weight and complexity over a conventional mechanical variable geometry exhaust system, a fixed geometry nozzle may be able to cover an entire flight envelope in some applications.

Nomenclature

A = nozzle area, in.^{2}
F = axial thrust, lb
M = Mach number
p = pressure, psi
T = temperature, °R
x = nozzle streamwise coordinate, in.
y = streamwise normal (vertical) coordinate, in.
α = flow angle, clockwise from horizontal, deg
β = oblique shock inclination angle, deg

Subscripts

a = ambient
e = nozzle exit
i = ideal
t = nozzle throat
0 = nozzle stagnation condition
1 = upstream of shock

I. Introduction

IN the world of modern fluid dynamics, boundary-layer separation is typically regarded as a "tragic" phenomenon and rightly so; performance penalties and instabilities often accompany separation, and these can have a detrimental or catastrophic effect on almost any fluid dynamic system. Putting this aside, however, it is important to realize that boundary-layer separation is a natural process; it is the means by which a viscous flow adjusts to its surroundings under particular conditions. In certain cases, this mechanism can have many benefits, ranging from enhanced performance to flow control.

Consider an overexpanded convergent–divergent (CD) nozzle. This condition occurs because the nozzle expansion ratio is too large for a given nozzle pressure ratio (NPR). Supersonic nozzle flow is driven to expand below exit backpressure, and a nonisentropic, discontinuous shock jump is required to adjust. Ideally, flow stays attached downstream of the shock, but in reality, it usually separates from the nozzle flap if the expansion ratio is high enough or the flap angle steep enough. Figure 1 shows flow in a shock-separated nozzle.

At first glance, it is often surprising that nozzle separation is accompanied by an increase in thrust efficiency over the attached case,[1] but it should not be surprising. A major effect of boundary-layer separation is that it redefines the "effective" geometry of a fluid dynamic system by displacing the inviscid flow. In a CD nozzle, separation moves the jet detachment point upstream, causing a change in the effective nozzle geometry to one that is shorter and has a lower expansion ratio. By acting like a natural adjustment mechanism, separation allows an overexpanded nozzle flow to reach a more efficient thermodynamic balance. For a given NPR, this alleviates overexpansion and improves thrust efficiency. Studies by Asbury et al.[2] and Hunter[3] showed that off-design nozzle thrust efficiency could be improved even further by encouraging stable separation (with a passive porous cavity) and controlling the location and extent of that separation. In addition, the studies demonstrated that effective thrust vectoring could be attained by asymmetric shock/boundary-layer interaction control.

Current aircraft typically use mechanical systems for nozzle area control and thrust vectoring. Although effective, these systems can be heavy, complex, expensive to maintain, and prone to fatigue and failure. They are also difficult to integrate aerodynamically and can be a primary source of drag. With the addition of other requirements such as infrared suppression, noise suppression, and low-observable shaping, the design and integration of an efficient mechanical exhaust system becomes all the more challenging.

The capabilities of future aircraft will depend on the development of simple, lightweight, multifunction exhaust systems that are aerodynamically efficient, compact, and inexpensive. In light of this, there is tremendous potential to improve aircraft system performance by replacing mechanical nozzle systems with efficient fixed-geometry configurations that use separation to enhance and control off-design performance. For this reason, and because of the complicated relationship between overexpansion, shock-induced separation, and thrust efficiency, an understanding of separated nozzle flows is critical and is the focus of the present work.

II. Experimental Arrangement

A. Static Test Facility

Experimental testing was conducted in the model preparation area of the NASA Langley Research Center 16-Foot Transonic Tunnel

Presented as Paper 98-3107 at the AIAA/ASME/SAE/ASEE 34th Joint Propulsion Conference and Exhibit, Cleveland, OH, 13 July 1998; received 15 August 2003; revision received 9 October 2003; accepted for publication 16 October 2003.

*Aerospace Engineer, Configuration Aerodynamics Branch, Mail Stop 499, 16 Victory Street; craig.hunter@nasa.gov.

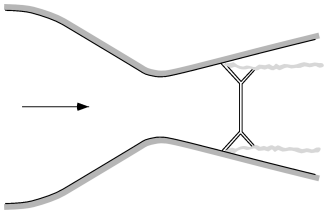

Fig. 1 Overexpanded CD nozzle with separation.

POINT	COORDINATES, IN. X	Y
A	0.000	0.000
B	0.000	-0.614
C	0.000	1.386
D	0.917	1.163
E	1.988	0.611
F	2.394	0.553
G	2.430	0.559
H	2.275	1.166
I	4.550	0.972

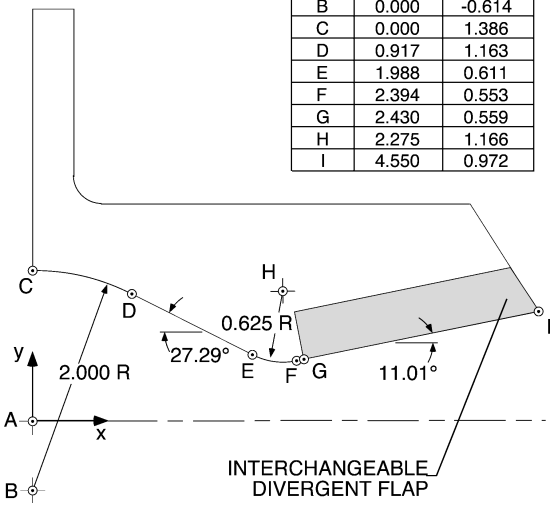

Fig. 2 Nozzle flap geometry.

Complex.[4,5] This facility is normally used for the buildup and calibration of wind-tunnel models, but can also be used for nozzle testing at static conditions. Models are mounted on a sting-strut support system in a 10×29 ft ambient test chamber and supplied with a regulated continuous flow of clean, dry air. A control room adjacent to the test chamber offers access through a soundproof door and observation window.

B. Test Nozzle

The test nozzle used in this investigation was a subscale, nonaxisymmetric, two-dimensional CD nozzle with a nominal throat area $A_t = 4.317$ in.^{2}, an expansion ratio $A_e/A_t = 1.797$, and a constant width of 3.990 in. Based on one-dimensional theory, the nozzle has a design NPR of 8.78 and an exit Mach number of $M_e = 2.07$. The nozzle was equipped with interchangeable divergent flaps to function as a testbed for various shock/boundary-layer interaction control concepts and had full-length optical-quality glass sidewalls to allow for internal flow visualization and flow diagnostic measurements. Geometric details of the nozzle flap are shown in Fig. 2, and a photograph of the nozzle is given in Fig. 3.

C. Propulsion Simulation System

High-pressure air was supplied to the test nozzle at a stagnation temperature of about $T_0 = 530°$R, with flow rates up to 15 lbm/s. As shown in Fig. 4, the propulsion simulation system uses choke points, plenums, turns, and flexible metal bellows to deliver air to a nozzle such that effects of momentum transfer and pressurization are minimized. This ensures that forces and moments produced by the nozzle can be accurately measured. Downstream of the flow transfer system, air passes through a circular-to-rectangular transition section, a choke plate, an instrumentation duct, and the test nozzle before exhausting to ambient backpressure.

D. Instrumentation

Airflow rates were calculated from pressure and temperature measurements in a multiple critical venturi located upstream of the

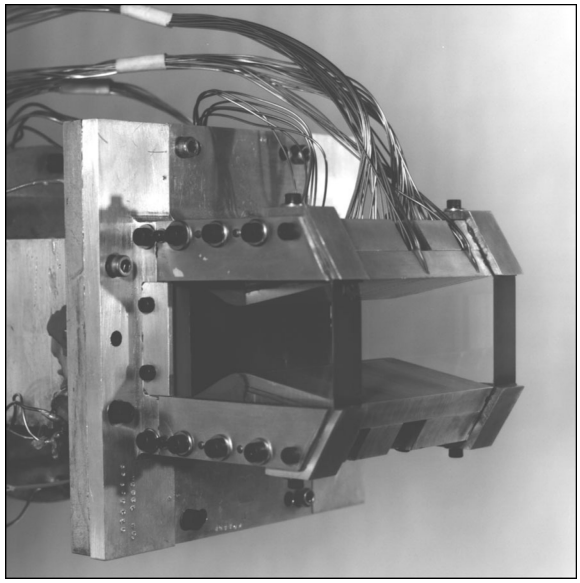

Fig. 3 Test nozzle.

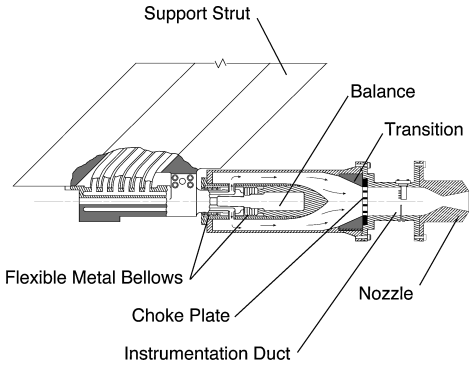

Fig. 4 Propulsion simulation system.

propulsion simulation system. Forces and moments were measured by a six-component strain-gauge balance located on the propulsion simulation system centerline (Fig. 4). Stagnation conditions were measured in the instrumentation duct using pitot tube rakes and pressure transducers for total pressure and iron–constantan thermocouples for total temperature. Surface static pressures were measured on the upper nozzle flap at the centerline (convergent and divergent flap) and at the sideline, 0.40 in. from the nozzle sidewall (divergent flap only). Pressure orifices were 0.020 in. in diameter and were connected to a combination of pressure transducers and an electronically scanning pressure module.

E. Data Acquisition and Reduction

Readings from the venturi, force balance, and pressure and temperature instrumentation were recorded simultaneously. Steady-state data were acquired by averaging 50 frames of instantaneous data sampled at rate of 10 frames/s. Calibration constants were applied to the raw data to obtain corrected forces, moments, pressures, and temperatures. A detailed description of the data reduction procedures used is given in Ref. 6.

The following conventions were used for data reduction: NPR is the ratio of nozzle total pressure p_0 to atmospheric backpressure p_a and was used to set test points. Thrust efficiency ratio F/F_i is the ratio of measured axial thrust F to ideal isentropic thrust F_i (calculated from the measured weight flow and stagnation conditions using one-dimensional theory). Normalized static pressure p/p_0 is the measured local static pressure p normalized by the nozzle total pressure p_0.

Nozzle testing was performed by taking 20 points of data over an NPR range from 1.25 to 9.5. These limits were established by

the lower and upper flow rates of the air supply system. To obtain detailed information on the overexpanded, shock-separated regime of the nozzle, 15 of the 20 data points were taken below NPR = 6.

F. Uncertainty Analysis

An uncertainty analysis was performed by propagating measurement bias uncertainties through the data reduction equations. This analysis assumes that bias errors dominate precision errors and is based on methods presented in Refs. 7 and 8. For the range of test conditions encountered in this study, the uncertainty of NPR and p/p_0 is approximately $\pm 0.28\%$ of measured value, and the uncertainty of F/F_i is approximately $\pm 0.4\%$.

G. Focusing Schlieren Flow Visualization

As data was acquired, a focusing schlieren system was used to visualize simultaneously internal nozzle flow. Based on criterion developed by Weinstein,[9] the schlieren system had a 133-mm-diam field of view, a sensitivity of 17 arc-s, a resolution of 0.25 mm, a depth of sharp focus of 4.6 mm, and a depth of unsharp focus of 36 mm. The light source for the schlieren system was a xenon strobe flash tube, driven at a 30-Hz rate with pulses of 0.6 μs duration and 0.05-W · s power. The system was focused on the test nozzle centerline plane and configured for sensitivity to streamwise density gradients. A 720×480 pixel resolution video camera and 70-mm Hasselblad still camera recorded results.

III. Theoretical Modeling

Theoretical predictions were made using NPAC.[10] NPAC uses an approximate theoretical method to calculate internal flow, thrust performance, and boundary-layer characteristics of two-dimensional CD nozzles. Internal flow and thermodynamic performance effects due to over- and underexpansion are modeled with one-dimensional compressible flow theory, and an approximate integral momentum method (based on the classic von Kármán–Polhausen solution) is used to calculate turbulent boundary-layer development and skin-friction losses. An iterative algorithm couples the boundary-layer solution to the one-dimensional flow model to correct for the effects of boundary-layer displacement on internal flow. Additional calculations account for exit flow angularity losses. The NPAC method has been well validated and is capable of predicting peak thrust efficiency to within 0.1% for a wide variety of two-dimensional CD nozzle shapes. For low expansion ratio nozzles, NPAC can generally predict off-design thrust efficiency to within 0.5%.

IV. Results

In this section, experimental results will be presented in terms of internal flow features (static pressure measurements and schlieren flow visualization) and thrust performance. Because the test nozzle had glass sidewalls that flexed slightly under pressurization, it was not possible to measure discharge coefficient accurately, and these data are not presented.

A. Internal Flow

Normalized experimental centerline static pressures p/p_0 vs nondimensional streamwise location relative to the nozzle throat are presented in Fig. 5. Results are representative of classic CD nozzle flow.[11] For the first data points at NPRs 1.25 and 1.4, pressure data indicate choked, internally overexpanded flow with a weak shock near the nozzle throat. Flow downstream of the shock appears to recover to ambient pressure $p/p_0 = 1/\text{NPR}$ in a smooth continuous fashion. Focusing schlieren flow visualization obtained at NPR = 1.4 is presented in Fig. 6 and shows a weak, almost normal shock downstream of the nozzle throat with little or no lambda foot structure evident. This shock/boundary-layer interaction is characteristic of a weak shock ($M_1 \approx 1.2$, estimated from p/p_0) and a thin boundary layer.

As seen in Fig. 5, the discontinuous nature of the pressure distribution at NPR = 1.6 indicates that the strength of the nozzle shock increased ($M_1 \approx 1.4$), and the inflection point in the recovery curve at $x/x_t = 1.3$ indicates that separation occurred, although it was not severe. By NPR = 1.8, the upstream shock Mach number was approximately $M_1 \approx 1.5$, and shock-induced separation began to significantly affect nozzle flow. At this NPR, there are strong signs of a separation bubble, with minimal pressure recovery from the shock location at $x/x_t = 1.3$ out to $x/x_t = 1.6$ and strong recovery occurring over the remaining length of the nozzle. Figure 7 shows the nozzle shock at NPR = 1.8 with a small lambda foot, as well as signs of unstable nozzle flow; the schlieren photograph imaged the shock in two positions over a 0.6-μs duration, indicating that the separation was unsteady.

As shown by pressure data in Fig. 5, an increase in NPR to 2.0 did not change shock location or strength, but flow fully detached and there was almost no pressure recovery downstream of the shock. This result is of critical importance because it serves to illustrate the

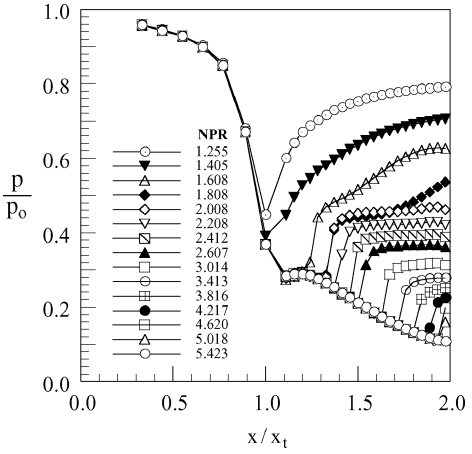

Fig. 5 Experimental centerline pressure data.

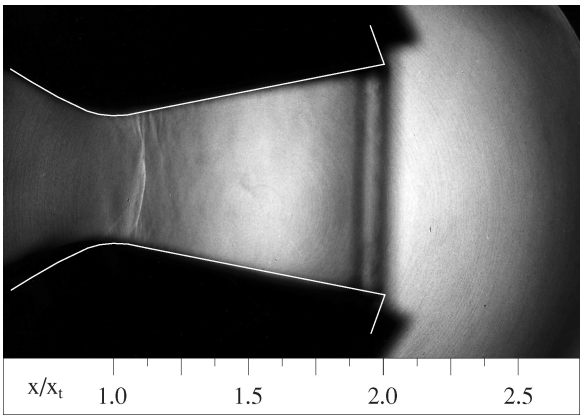

Fig. 6 Schlieren flow visualization at NPR = 1.4.

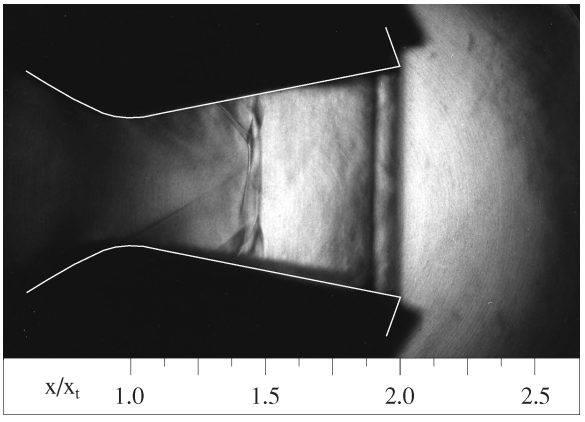

Fig. 7 Schlieren flow visualization at NPR = 1.8.

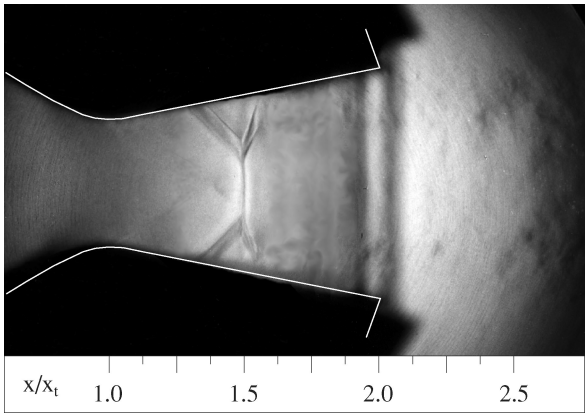

Fig. 8 Schlieren flow visualization at NPR = 2.0.

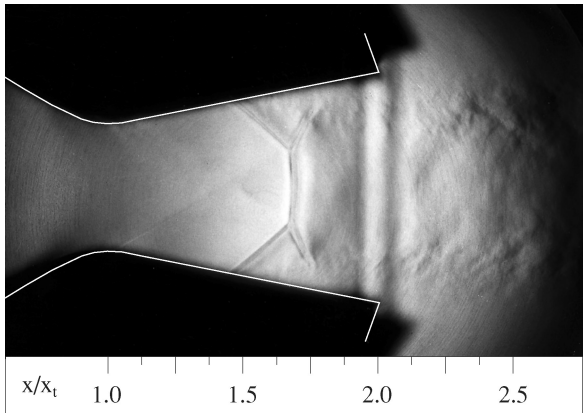

Fig. 9 Schlieren flow visualization at NPR = 2.4.

relationship between NPR, shock/boundary-layer interaction and separation. For this NPR, nozzle flow adjusted to exit conditions by completely detaching past the shock; internal conditions up to and through the shock were nearly identical to those of the earlier NPR. Thus, separation that occurred at NPR = 2.0 was probably not the result of a stronger shock/boundary-layer interaction, but instead came about through the natural tendency of an overexpanded nozzle flow to separate, thereby adjusting to a lower expansion ratio geometry. Among other things, this suggests that the shock/boundary-layer interaction is not so much the cause of separation, but is more of a mutually dependent result.

Schlieren flow visualization at NPR = 2.0 in Fig. 8 shows the nozzle shock with a pronounced lambda foot system and fully detached separation extending from the leading lambda shock downstream past the nozzle exit. That the appearance of a large lambda foot coincided with the onset of fully detached separation inside the nozzle is an important observation because it shows that the size and extent of a lambda foot is more a result of separation effects than it is of basic shock/boundary-layer interaction conditions such as onset Mach number or boundary-layer state. This makes sense; a fully detached region would impose stronger turning requirements on nozzle flow than a closed separation bubble and would require a bigger oblique shock system. As the separation point became the effective nozzle exit, the lambda shock system adjusted to satisfy continuity of pressure and flow direction in the new effective geometry.

Fully detached separation occurred for subsequent NPRs past 2.0. Figure 9 shows the shock at NPR = 2.4 with a well-defined lambda foot and separation, and Fig. 10 shows the same at NPR = 3.0. By NPR = 3.4, the lambda shock foot had grown significantly, such that the main shock and trailing lambda foot were outside the physical nozzle, as shown in Fig. 11. At this NPR, flow past the separation point showed strong resemblance to externally overexpanded flow; the jet plume necked down between the leading and trailing lambda foot, and there was an expansion fan emanating from each trailing lambda foot as it intersected the free shear layer. This indicates that,

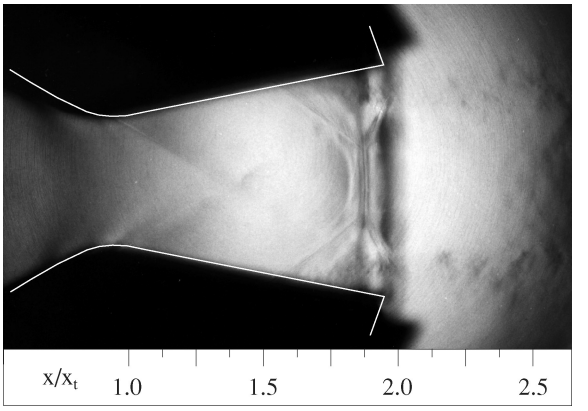

Fig. 10 Schlieren flow visualization at NPR = 3.0.

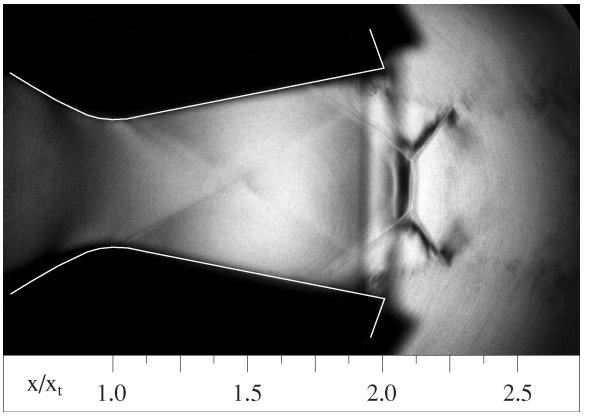

Fig. 11 Schlieren flow visualization at NPR = 3.4.

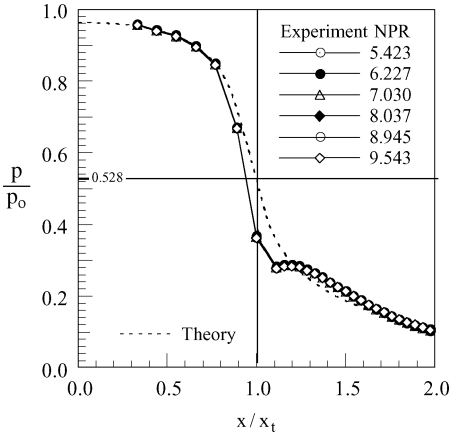

Fig. 12 Centerline pressures for NPR $\geq$ 5.4.

not only was the separation point behaving like the nozzle exit, but also flow past this point was overexpanding externally, which would occur in a lower expansion ratio nozzle at the same NPR.

The leading lambda foot worked its way out of the nozzle with increasing NPR, and pressure data in Fig. 5 show the nozzle to be shock free by NPR = 5.4. As shown in Fig. 12, pressures fell on the same curve above NPR = 5.4, which indicated that internal flow was independent of NPR in this range. When experimental data is compared with a theoretical pressure distribution, one feature clearly evident in Fig. 12 is the vena contracta effect, which occurs when acceleration causes flow to overshoot the nozzle throat radius. This causes flow to reach sonic velocity upstream of the geometric throat and leads to local overexpansion and compression, evidenced by the dip and bump in pressure data from $x/x_t \approx 0.8$ to $x/x_t \approx 1.5$. High-sensitivity schlieren flow visualization at NPR = 8.95 (near design) is presented in Fig. 13 and shows the skewed, bell-shaped sonic line

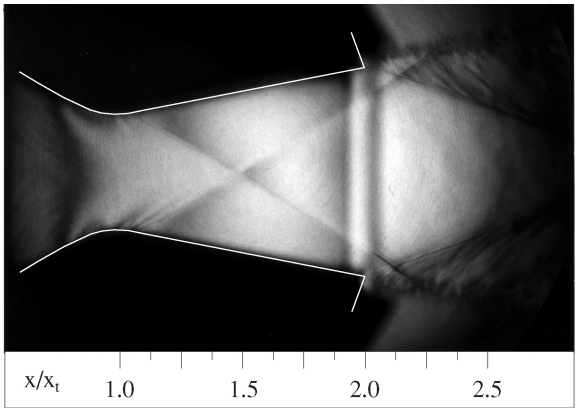

Fig. 13 Schlieren flow visualization at NPR = 8.95.

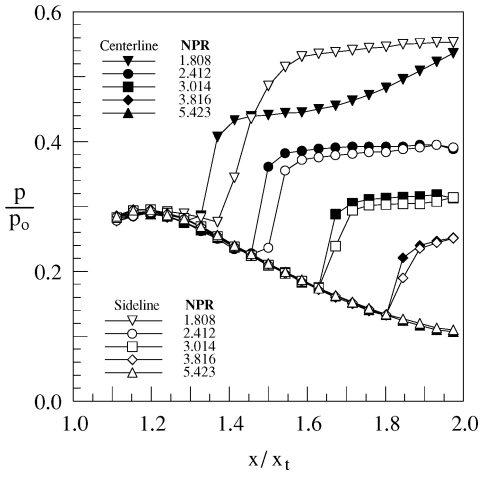

Fig. 14 Centerline–sideline pressure comparison.

(dark band) upstream of the geometric nozzle throat, the local overexpansion (dark regions) near the throat, and oblique shocks marking the recompression. These features were present for all NPRs above 1.6.

Experimental divergent flap sideline pressures are compared to centerline pressures at selected NPRs in Fig. 14. At NPR = 1.8, there are noticeable differences between sideline and centerline pressure in terms of shock location and downstream pressure recovery, indicating that nozzle flow was highly three-dimensional and the shock was nonplanar. For NPR = 2.4 and above, sideline and centerline exit pressures were equal, and by NPR = 3.0, sideline and centerline shock locations became nearly equal and remained that way for all higher NPRs, which indicated that flow was well behaved and nearly two dimensional. At NPR = 5.4 (shock free nozzle), sideline and centerline pressures fall on the same curve.

B. Performance

Thrust efficiency results are shown in Fig. 15, where the measured thrust ratio F/F_i is plotted vs NPR and accompanied by a theoretical curve (computed by NPAC) for comparison. Near the design pressure ratio of 8.78, measured thrust efficiency reached a maximum of $F/F_i = 0.986$, which is consistent with the 0.985–0.990 range reported in other studies[12,13] and in agreement with the theoretical prediction. This indicates that on-design losses were likely due to the same effects modeled by NPAC at this fully expanded condition: skin friction, boundary-layer displacement, and flow angularity.

Below the design point of the nozzle, measured thrust efficiency decreased, closely following the theoretical prediction down to about NPR = 4.6. Again using the NPAC model for guidance, this indicates that internal performance effects and losses were constant in this range and that thrust efficiency was governed by the thermodynamics of flow in an overexpanded CD nozzle. The fact that this agreement extended down to NPR = 4.6 correlates well with pressure data that indicated the nozzle was approaching a shock free condition near this point.

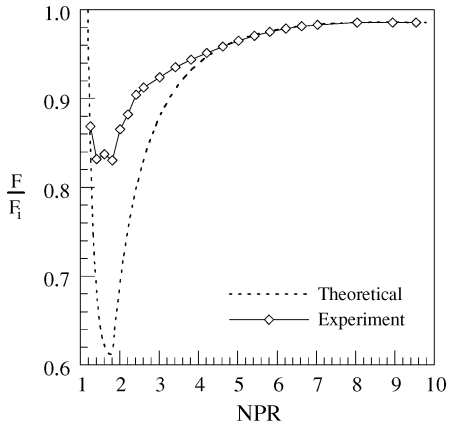

Fig. 15 Experimental and theoretical thrust efficiency.

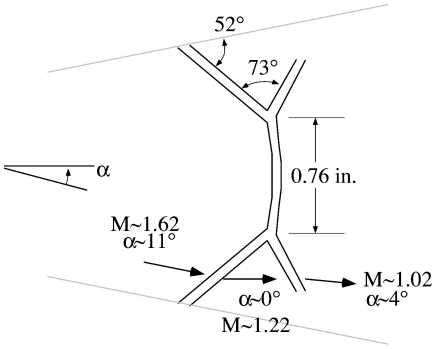

Fig. 16 Shock schematic at NPR = 2.4.

Below NPR = 4.6, measured thrust efficiency rose above the theoretical prediction and remained there for all lower NPRs before returning to the theoretical curve at NPR = 1.25. At its best point, measured thrust efficiency showed a 22% increase over theoretical thrust efficiency at NPR = 1.6. As supported by earlier discussion, this behavior corresponds to the fact that shock-induced boundary layer separation was altering the effective nozzle geometry to one with a more efficient, lower expansion ratio. This was most noticeable at lower NPRs where the nozzle shock was farther upstream and separation had a bigger effect on nozzle flow and the effective expansion ratio.

Several other observations round out this discussion. First, just as the high end departure from the theoretical curve occurred at NPR = 4.6 due to the "end" of separated flow, the low end departure from the theoretical curve occurred around NPRs 1.4–1.8, where early stages of separation were present. Note that measured F/F_i was nearly constant in this range because the nozzle was going through stages of transitory separation. In addition, the marked increase in measured F/F_i as NPR went from 1.8 to 2.0 corresponds to the onset of fully detached separation in the nozzle and represents the single largest NPR to NPR leap in thrust efficiency measured (as evidenced by the slope of the F/F_i curve), an increase of 3.5%. Obviously, this confirms the that the nozzle flow went through a dramatic change at this point.

C. Shock Schematic at NPR = 2.4

Geometrical shock measurements were made from the experimental schlieren image and used in conjunction with pressure data and oblique shock relations[11] to diagram the shock/boundary-layer interaction at NPR = 2.4. (This NPR was chosen because of the well-defined schlieren image available.) As shown in Fig. 16, the leading lambda shock had a flow inclination angle $\beta \approx 52$ deg from the nozzle flap, which, with an upstream Mach number of $M_1 \approx 1.6$, resulted in a calculated turning angle of 11 deg and a downstream Mach number of approximately 1.2. From this new direction, the

trailing shock had an inclination of $\beta \approx 66$ deg, and with $M_1 \approx 1.2$, the corresponding turning angle was 4 deg. Overall, this indicates that flow exited the lambda shock system at an angle of $\alpha \approx 4$ deg, or 7 deg off of the divergent flap.

V. Conclusions

An experimental investigation of separated nozzle flows has been conducted. Results indicate that the test nozzle was dominated by shock-induced boundary-layer separation at overexpanded off-design conditions. This separation had two distinct regimes: for NPR ≤ 1.8, the separation was three dimensional, somewhat unsteady, and confined to a bubble (with partial reattachment over the nozzle flap). For NPR ≥ 2.0, separation was steady and fully detached, and it became more two dimensional as NPR increased. When NPR increased from 1.8 to 2.0, the nozzle went through a dramatic transition, dividing the two separated flow regimes. In all cases, separation improved static thrust efficiency when compared to the ideal (attached flow) theoretical model. As the nozzle became shock free, thrust efficiency followed along the theoretical prediction and matched the theoretical peak thrust efficiency.

The transition from partial separation to fully detached separation observed when NPR was increased from 1.8 to 2.0 resulted in several important observations. With this NPR increase, nozzle flow adjusted to exit backpressure by completely detaching downstream of the shock; conditions up to the shock were nearly the same as the earlier NPR. Thus, this transition was not the result of markedly different onset conditions or a stronger shock/boundary-layer interaction, but instead came about through the natural tendency of an overexpanded nozzle flow to detach and reach a more efficient thermodynamic balance. This suggests that in nozzle flows, shock/boundary-layer interaction and separation are mutually dependent results, in contrast to the typical view that shock/boundary-layer interaction is the cause of separation.

These results illustrate potential benefits of encouraging stable separation in an exhaust nozzle. With the entire overexpanded range of nozzle performance within 16% of the peak thrust efficiency, a fixed-geometry nozzle may be able to cover an entire flight mission more efficiently than a mechanical variable-geometry system due to reductions in weight and complexity. Of course, external flow and aerodynamic effects also need to be taken into consideration in any potential application.

References

[1]Lewis, W. G. E., "Propelling Nozzle Research," *Journal of the Royal Aeronautical Society*, Vol. 68, Nov. 1964, pp. 717–727.

[2]Asbury, S. C., Gunther, C. L., and Hunter, C. A., "A Passive Cavity Concept for Improving the Off-Design Performance of Fixed-Geometry Exhaust Nozzles," AIAA Paper 96-2541, July 1996.

[3]Hunter, C. A., "An Experimental Analysis of Passive Shock–Boundary Layer Interaction Control for Improving the Off-Design Performance of Jet Exhaust Nozzles," M.S. Thesis, Joint Institute for Advancement of Flight Sciences, George Washington Univ., Washington, DC, Sept. 1993.

[4]Propulsion Aerodynamics Branch Staff, "A User's Guide to the Langley 16-Foot Transonic Tunnel Complex, Revision 1," NASA TM-102750, Sept. 1990.

[5]Capone, F. J., Bangert, L. S., Asbury, S. C., Mills, C. T., and Bare, E. A., "The NASA Langley 16-Foot Transonic Tunnel: Historical Overview, Facility Description, Calibration, Flow Characteristics, and Test Capabilities," NASA TP-3521, Sept. 1995.

[6]Mercer, C. E., Berrier, B. L., Capone, F. J., and Grayston, A. M., "Data Reduction Formulas for the 16-Foot Transonic Tunnel at NASA Langley Research Center, Revision 2," NASA TM-107646, July 1992.

[7]Coleman, H. W., and Steele, W. G., Jr., *Experimentation and Uncertainty Analysis for Engineers*, Wiley, New York, 1989, Chap. 1–7.

[8]Wing, D. J., Mills, C. T. L., and Mason, M. L., "Static Investigation of a Multiaxis Thrust-Vectoring Nozzle With Variable Internal Contouring Ability," NASA TP-3628, June 1997.

[9]Weinstein, L. M., "An Improved Large-Field Focusing Schlieren System," AIAA Paper 91-0567, Jan. 1991.

[10]Hunter, C. A., "An Approximate Theoretical Method for Modeling the Static Thrust Performance of Non-axisymmetric Two-Dimensional Convergent-Divergent Nozzles," NASA CR-195050, March 1995.

[11]Anderson, J. D., *Modern Compressible Flow with Historical Perspective*, McGraw–Hill, New York, 1982, Chap. 5.

[12]Capone, F. J., Konarski, M., Stevens, H. L., and Willard, C. M., "Static Performance of Vectoring/Reversing Non-axisymmetric Nozzles," AIAA Paper 77-840, July 1977.

[13]Leavitt, L. D., "Summary of Nonaxisymmetric Nozzle Internal Performance from the NASA Langley Static Test Facility," AIAA Paper 85-1347, July 1985.